PHYSICAL REVIEW FLUIDS **2**, 064608 (2017)

Skewness and flatness factors of the longitudinal velocity derivative in wall-bounded flows

Lyazid Djenidi* and Robert A. Antonia
Discipline of Mechanical Engineering, School of Engineering, University of Newcastle, Newcastle, NSW 2308, Australia

Murali K. Talluru
Discipline of Civil Engineering, University of Sydney, Sydney, NSW 2006, Australia

Hiroyuki Abe
Japan Aerospace Exploration Agency, Tokyo 182-8522, Japan
(Received 5 March 2017; published 28 June 2017)

Hot-wire measurements are carried out in turbulent boundary layers over smooth and rough walls in order the assess the behavior of the skewness (S) and flatness (F) factors of the longitudinal velocity derivative as y, the distance from the wall, increases. The measurements are complemented by direct numerical simulations of a smooth wall turbulent channel flow. It is observed that, as the distance to the wall increases, S and F vary significantly before approaching a constant in the outer layer of the boundary layer. Further, S and F exhibit a nontrivial dependence on the Taylor microscale Reynolds number (Re_λ). For example, in the region below about 0.2δ (δ is the boundary layer thickness) where Re_λ varies significantly, S and F strongly vary with Re_λ and can be multivalued at a given Re_λ. In the outer region, between 0.3δ and 0.6δ, S, F, and Re_λ remain approximately constant. The channel flow direct numerical simulation data for S and F exhibit a similar behavior. These results point to the ambiguity that can arise when assessing the Re_λ dependence of S and F in wall shear flows. In particular, the multivaluedness of S and F can lead to erroneous conclusions if y/δ is known only poorly, as is the case for the atmospheric shear layer (ASL). If the laboratory turbulent boundary layer is considered an adequate surrogate to the neutral ASL, then the behavior of S and F in the ASL is expected to be similar to that reported here.

DOI: 10.1103/PhysRevFluids.2.064608

I. INTRODUCTION

The atmospheric shear layer (hereafter denoted ASL) data played a pivotal role in testing small-scale statistics within the framework of both Kolmogorov's original 1941 theory (K41) [1,2] and its revision (K62) [3]. In particular, these data have been used [4] to assess the Reynolds number dependence of both S and F (the skewness and flatness factor, respectively, of $\partial u/\partial x$, u is the longitudinal velocity fluctuation). In the framework of K41, S and F should be independent of the Taylor microscale Reynolds number $\mathrm{Re}_\lambda = u'\lambda/\nu$ (λ is the Taylor microscale, ν the fluid kinematic viscosity, and the prime denotes the rms), while under K62 they are generally expected to increase with Re_λ. The ASL data reported in Ref. [4] conformed with the latter trend. However, one critical issue relating to these ASL data which may cast doubts on their suitability for testing K41 and K62 is that the measurements were carried out at relatively small heights above the ground or ocean surface, and were therefore influenced by near-surface effects. As the surface is approached, the individual contributions of the various physical mechanisms (i.e., production, advection, turbulent

*lyazid.djenidi@newcastle.edu.au

and viscous diffusion, and pressure-velocity diffusion) to the turbulent kinetic energy change from those away from the surface. Further, the lack of knowledge of the ASL thickness prevents one from assessing whether or not the heights at which the measurements were carried out are large enough for neglecting the near-surface effects. Another issue of relevance when testing K41 and K62 relates to the "state" (stable, unstable, or neutral) of the ASL. The ASL should exhibit neutral stratification to be comparable to most laboratory data, i.e., the Monin-Obukhov length [5] should be infinitely large or, at least, very large, to avoid the effects of buoyancy. Interestingly, in his review of atmospheric turbulence, Wyngaard [6] states that he knew of no measurements in a truly neutral boundary layer, one with zero buoyancy flux. It should be also remembered that the ASL is subjected to a pressure gradient and to the Coriolis force; this latter is often assumed to be weak.

Finally, so far the possibility that S and F in the ASL could, in addition to being Re dependent, also depend on the distance to wall was ignored or overlooked. Clearly, this possibility needs to be investigated, which is the aim of the present study. Ideally, measurements across the entire neutral ASL should be carried out in order to assess (i) whether or not the ASL, as data reported, for example, in Ref. [4], are free of any near-wall effects and (ii) if the behavior of S and F changes with distance from the ground surface. Unfortunately, such measurements are not possible in the ASL. However, it is commonly assumed that the laboratory boundary layer can be a relatively good surrogate for the neutral ASL (e.g., Refs. [7,8]). Only a few studies have reported distributions of S and F across a turbulent boundary layer (e.g., Ref. [9]). They show that S and F vary as the distance to the wall is approached. This is also observed in a turbulent pipe flow [10] and a turbulent channel flow [11].

The present paper reports measurements of laboratory smooth and rough wall turbulent boundary layers as well as direct numerical simulation (DNS) data in a smooth wall turbulent channel flow. The study assesses the behaviors of S and F in turbulent wall shear flows, and in particular their behavior as the distance to the wall varies. This should help determine the suitability of the ASL data for S and F reported in Ref. [4] for testing K41 and K62. Although it is generally accepted that there are severe difficulties in carrying out measurements in an often uncontrolled environment such as the ASL, we are not leveling any criticism at the measured values of S and F in the ASL reported in Ref. [4]. These measurements were obtained with care and most likely reflect the true state of the ASL at the locations where the data were acquired. Our study assesses how, as the wall is approached, the increase in the mean shear and anisotropy can affect the distributions of S and F with the assumption that these distributions are similar to those in the ASL.

II. DETAILS OF EXPERIMENTS AND NUMERICAL SIMULATIONS

Hot-wire experiments are conducted in smooth and rough wall boundary layer wind tunnels located at the University of Newcastle. The smooth wall wind tunnel, previously documented by Ref. [12], has a test section of 4.0 m length and 0.825 m width. It has a height of 0.16 m at the exit of contraction (9.5:1). The boundary layer is tripped by a 100-mm-long roughness strip of No. 40 grit sandpaper. The roof height in the test section is adjusted to obtain a nominally zero pressure gradient turbulent boundary layer. For all the experiments presented here, the coefficient of pressure along the entire working section is maintained constant to within $\pm 0.5\%$. It was verified by Ref. [12] that the boundary layer behaved according to the criteria for fully developed turbulent boundary layers. Measurements are carried out at four streamwise locations x, ranging between $1.15\ \text{m} \leqslant x \leqslant 2.6\ \text{m}$ downstream of the trip at a nominal free stream velocity of 10 m/s. However, for the purpose of the present study, only the measurements at $x = 2.6$ m are used in order to have a direct comparison with rough wall measurements at $x = 2.54$ m (details given below). In all the smooth wall measurements, the friction velocity U_τ was obtained by fitting the logarithmic mean velocity profile to the constants $\kappa = 0.384$ and $A = 4.17$ [13]. The Reynolds number $\text{Re}_\tau = \delta U_\tau/\nu$ (where ν is the kinematic viscosity) ranges between 900 and 1500.

The rough wall wind tunnel is the same as the one used in the previous studies of Refs. [14,15]. The advantage of using a rough wall is that it can produce higher Reynolds number turbulent boundary layers than a smooth wall in a low-speed wind tunnel. The test section is 5.4 m long

and 0.9 m wide. At the exit of the contraction (6:1), the test section has a height of 0.15 m. It is tripped at the contraction exit by a 4-mm-diam rod followed by a 170-mm-long strip of No. 40 grit sandpaper. Following the contraction, the roof of the test section is adjusted in order to compensate for the growth of the boundary layers and to maintain the pressure gradient within $\pm 0.1\%$ of the free-stream dynamic pressure. The rough wall consisted of a periodic arrangement of cylindrical rods mounted only on the bottom wall and spanning across the full width of the test section. The diameter of the rods (k) is nominally 1.6 mm and the spacing p between the rods is set at $p = 8k$. Measurements are made at 2.54 m downstream of the tripped inlet of the working section. The free-stream velocity U_∞ is varied between 2 and 19 ms^{-1}. The boundary layer thickness (δ_{99}, hereafter δ) is found to be nominally 0.1 m (about $63k$). The friction velocity U_τ is obtained by integrating the pressure distribution around a roughness element (see Ref. [15] for full details). The Reynolds number $\mathrm{Re}_\tau = \delta U_\tau/\nu$ (where ν is the kinematic viscosity) ranges between 620 and 7200.

In all the rough wall experiments, a total of 36 logarithmically spaced measurement points between $y = 0.2$ and 136 mm (y is the wall-normal distance) are taken using the Mitutoyo height gauge with a resolution of 0.01 mm. The traversing system is also fitted with an optical linear encoder with a resolution of 1 μm, which improved the accuracy of positioning the hot-wire probe relative to the wall. Throughout this paper, x and y refer to the streamwise and wall-normal directions, respectively, while u denotes the fluctuating streamwise velocity component.

A. Hot-wire anemometry

The hot-wire probe used in all the experiments is a slightly modified Dantec 55P15 boundary layer type probe and has a spacing of 1.5 mm with a 2.5-μm-diam platinum Wollaston wire soldered between the prongs. The wire is etched to a length of 0.52 mm to ensure a length-to-diameter ratio $l/d \approx 210$. This equates to an inner-normalized sensor length l^+ of approximately 13 and 30 for smooth and rough wall measurements, respectively. The hot wire is operated using a in-house made constant temperature anemometer (CTA) with an overheat ratio of 1.8. The overall system response is found to be second order when a 1 kHz electronic square wave is applied to the CTA system and the -3 dB drop-off point corresponds to 16–30 kHz for mean velocities in the range 0–20 m/s. We used Taylor's hypothesis of frozen turbulence in the form $(\partial/\partial x) = -(1/U)(\partial/\partial t)$ to compute the velocity derivative $\partial u/\partial x$.

Calibration of the hot wire is carried out statically against a pitot-static tube located in the undisturbed free stream before and after every experiment at 16 different speeds ranging between 0 and 19 ms^{-1}. The pitot-static tube is connected to a micromanometer FC0332 from Furness Controls with an accuracy of 0.0125 Pa (0.025% full scale output) in the range of 0–00 Pa. A third-order polynomial is fitted between the free-stream velocity and the hot-wire voltage during the calibration. A linear interpolation in time between pre- and postcalibrations (see Ref. [16] for details) is employed to account for any drift in the hot-wire voltage that occurs during the course of an experiment. Only a minor drift of less than 0.1 V in hot-wire voltage was observed in our experiments.

The hot-wire signals were filtered using a low-pass analog filter before they were digitized using a 16-bit National Instruments NI9215 module installed on a NI cDAQ-9174 analog-to-digital converter. The filter cutoff frequency $f_c(y)$ is varied across the boundary layer so as to resolve the smallest scales at a given wall-normal location and the data are sampled at more than twice $f_c(y)$ for about 180 s.

B. Direct numerical simulation

The present numerical database was obtained from the direct numerical simulation (DNS) of a smooth wall turbulent channel flow with passive scalar transport [17]. Three values of h^+ (=180, 395, and 640) are used. The numerical methodology is briefly described as follows. A fractional step method is used with semi-implicit time advancement. The third-order Runge-Kutta method is employed for the viscous terms in the wall-normal (y) direction and the Crank-Nicolson method is used for the other terms. A finite difference method is adopted for spatial discretization.

TABLE I. Experimental details of smooth and rough wall measurements. Note that the black square in this table corresponds to green squares in the figures for better visibility.

x (m)	Re_τ	Re_θ	U_∞ (ms^{-1})	ν/U_τ (μm)	U_τ (ms^{-1})	δ_{99} (m)	δ^* (m)	θ (m)	l^+	k_s^+	δ/k	Symbol
Smooth wall												
2.6	1420	3540	9.7	41.0	0.378	0.058	0.0081	0.0057	12.2			■
Rough wall												
2.54	629	1760	2.07	142	0.108	0.089	0.022	0.013	3.5	47	56	◯
2.54	1020	2750	3.03	92.8	0.166	0.094	0.024	0.014	5.4	103	59	◊
2.54	1516	3922	4.17	64.6	0.238	0.098	0.026	0.015	7.7	220	61	△
2.54	2340	6045	6.43	41.0	0.381	0.096	0.026	0.015	12.2	299	62	□
2.54	3945	9925	10.40	25.1	0.623	0.099	0.026	0.015	19.8	450	62	×
2.54	5766	14305	15.00	17.4	0.900	0.100	0.025	0.015	28.7	625	63	∗
2.54	7170	17780	18.80	14.0	1.127	0.101	0.025	0.015	35.6	767	63	+

A fourth-order central scheme [18] is used in the streamwise (x) and spanwise (z) directions, with a second-order central scheme in the y direction. The velocity derivative $\partial u/\partial x$ is thus calculated with the use of a fourth-order central scheme. Periodic boundary conditions are applied in the x and z directions, whereas the no-slip condition is used in the y direction. A uniform grid distribution is used in the x and z directions, while a nonuniform distribution is used in the y direction where the grid is clustered near the wall but stretched towards the center of the channel. Special care is taken for the spatial resolution. The grid spacing in the x and z directions (Δx and Δz) is about 0.8 times the Kolmogorov length scale [17], which is similar to that of Ref. [11] who examined small-scale velocity pressure fluctuations by performing DNS with a well-resolved spatial resolution. On the other hand, the grid spacing in the y direction (Δy) is about 1.6 times the Kolmogorov length scale at the channel centerline; it is comparable to that of Ref. [19] who made a well-established DNS database up to $h^+ = 2003$. It is, however, about twice as coarse as that of Ref. [11]. Further details of the simulation are given in Ref. [17], and the reader may refer to this paper for information on basic turbulence statistics.

III. RESULTS

Although not shown here, the present data for the mean velocity and turbulence intensity distributions support the argument that a laboratory turbulent boundary layer (hereafter denoted LTBL) share similar features with the neutral ASL. This corroborates the results of Ref. [8]. One may thus expect that the behavior of the turbulence statistics across the LTBL reflects those of the ASL. In particular, for the problem that concerns us here, the distributions of S and F in the LTBL should mimic those in the ASL. This is of great interest as it allows us to better interpret the measured S and F in the ASL. In the next section we examine the distributions of S and F in the LTBL and the DNS of the turbulent channel flow.

A. Skewness and flatness of $\partial u/\partial x$

Figure 1 shows the measured distributions of S as function of y/δ and y^+ in the LTBL over the smooth and rough walls, and the DNS distributions in a smooth wall turbulent channel flow. Also shown are S for a smooth wall LTBL [9], smooth wall turbulent pipe [10], and the DNS of a smooth wall turbulent channel flow reported by Ref. [11].

All the distributions of S in Fig. 1 are qualitatively similar in all the smooth wall flows, with minor quantitative variations. As the distance to the wall increases, S first decreases, reaches a minimum, increases, and finally becomes constant over a large part of the outer region of the flow, forming a plateau. Note the systematic shift to smaller y/δ of the local minimum in S, reflecting

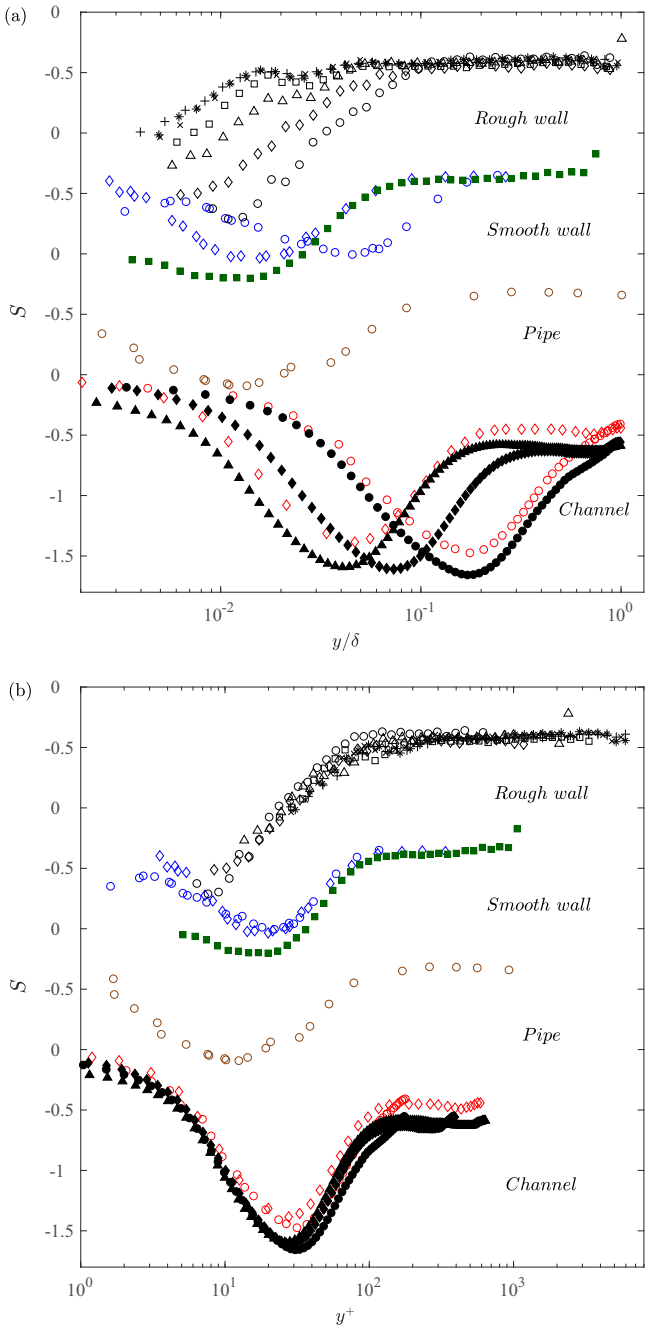

FIG. 1. Velocity derivative skewness S in a pipe, channel flow, and turbulent boundary layers as a function of (a) y/δ and (b) y^+. Open black symbols (see Table I): Rough wall boundary layer (current study). Blue symbols: Smooth wall boundary layer [9]. Green squares: Smooth wall boundary layer (Newcastle). Brown open circles: Pipe flow ($R^+ = 925$ [10]). Red open symbols: Channel flow DNS data ($h^+ = 180$,590 [11]). Black solid symbols: Present DNS channel flow data ($h^+ = 180$, 395, and 640). For the pipe and channel, δ stands the pipe radius (R) or channel half width (h), respectively. Note that the data for pipe, smooth, and rough wall turbulent boundary layers are represented using multiple ordinate axes.

the increase of Re. We used a semilog scale for the wall-normal coordinate to highlight this shift. Near the edge of the LTBL or the channel centerline, S tends to deviate from the plateau. On the plateau, S is about -0.4 for smooth and rough LTBLs and about -0.3 in the pipe. There is a vertical shift in the channel flow distributions between the present DNS and those of Ref. [11], which we cannot yet explain. The value of the plateau is different: -0.6 for our results and -0.4 for Ref. [11]. For the rough wall, S increases initially before reaching a constant value of about -0.4. Since the wall boundary configuration is different from that of a smooth wall, thus affecting the turbulence structure, the behavior of S in the vicinity of the wall differs from that of a smooth wall. When we use the inner-normalized distance y^+, we observe that the location of the minimum value of S on the smooth wall occurs at about $y^+ \simeq 20$–30; for the pipe it is at about $y^+ \simeq 10$–15. These positions are relatively close to the average location of the centroid of the quasilongitudinal vortices. On the rough wall, these vortices are absent at the higher Re, but they may occur at the lowest Re, when the boundary layer is in a transitionally rough regime.

We also observe a characteristic behavior of F in all smooth wall flows (Fig. 2). For example, as y^+ increases, F decreases, reaches a minimum, then increases to a maximum before finally decreasing towards a constant. On the rough wall, F shows a continuous decrease until it reaches a plateau. As S, F deviates from the plateau as the edge of the boundary layer or the centerline of the channel and pipe is approached. The value of F on the plateau is about 6 for both boundary layers and the channel flow and for the pipe it is about 3.

We now assess the behavior of S and F in terms of Re_λ [$\lambda \equiv u'/\overline{(\partial u/\partial x)^2}^{1/2}$] across the boundary layer and the channel flow (Fig. 3). To help visualize the Re_λ dependence of S across the flow, we color coded some S and Re_λ distributions and used different colors to identify various regions of the boundary layer. The inset of Fig. 3 shows the two Re_λ distributions corresponding to the color-coded distributions of S. Re_λ varies significantly as the wall is approached, but remains approximately constant in the region $0.2 \leqslant y/\delta \leqslant 0.6$; on the smooth wall, Re_λ exhibits a near-wall maximum which reflects the near-wall peak of u'. This behavior of Re_λ is observed at all Reynolds numbers Re_θ, as seen in Fig. 4, which reports the distributions of Re_λ as a function of y/δ for the smooth and rough wall turbulent boundary layers and the (DNS) smooth wall channel flow. The drop in Re_λ as the edge of the boundary layer is approached reflects the strong large-scale intermittency at the interface between the boundary layer and the potential flow.

For the smooth wall, the distributions of S and F in Fig. 3 show a nontrivial Re_λ dependence, in particular, in the near-wall region (e.g., red symbols), where both distributions exhibit a cusp when Re_λ reaches its local maximum. Farther away from the wall, S becomes independent of Re_λ for both the boundary layer and the channel flow. The distributions of F also exhibit a similar behavior with Re_λ. The near-wall behaviors of S and F on the rough wall differ from those on the smooth wall because the roughness alters significantly the near-wall turbulent structure of the flow. Further, as Re_θ (θ is the LBTL momentum thickness) increases, the independence of S on Re_λ, as the distance y increases, becomes clearer. For example, S is practically constant for the range $100 \leqslant \mathrm{Re}_\lambda \leqslant 170$ when $\mathrm{Re}_\theta = 2750$; when $\mathrm{Re}_\theta = 17\,780$ that range becomes $100 \leqslant \mathrm{Re}_\lambda \leqslant 500$. A similar trend is displayed by F.

The deviation from the plateau in both S and F as the wall is approached (e.g., Figs. 1 and 2) reflects most certainly the strong anisotropy in the near-wall region of wall-bounded flows, where several mechanisms are at play in the energy budget (e.g., production, dissipation, turbulent diffusion, transfer of pressure-velocity correlation). This alteration of the energy budget is also accompanied by a strong variation of Re_λ. In contrast, in the outer region, especially where $\mathrm{Re}_\lambda \simeq$ const the energy budget is dominated by the production and the dissipation, indicating an energy equilibrium. This equilibrium is expected to be matched at small scales by a balance between production and destruction of enstrophy $\overline{\omega_i \omega_i}$ (ω_i is the vorticity fluctuations; the repeated subscript implies summation over $i = 1$, 2, and 3). Further, local isotropy is likely to be relatively well satisfied in regions of weak or zero mean shear flow [20] and where Re_λ is expected to vary weakly or be constant. This occurs in the outer region of the flow, as already seen in Fig. 4.

The above results strongly suggest that caution is required when comparing S and F between wall turbulent flows and either decaying shear flows, such as jets and wakes, or homogeneous turbulent

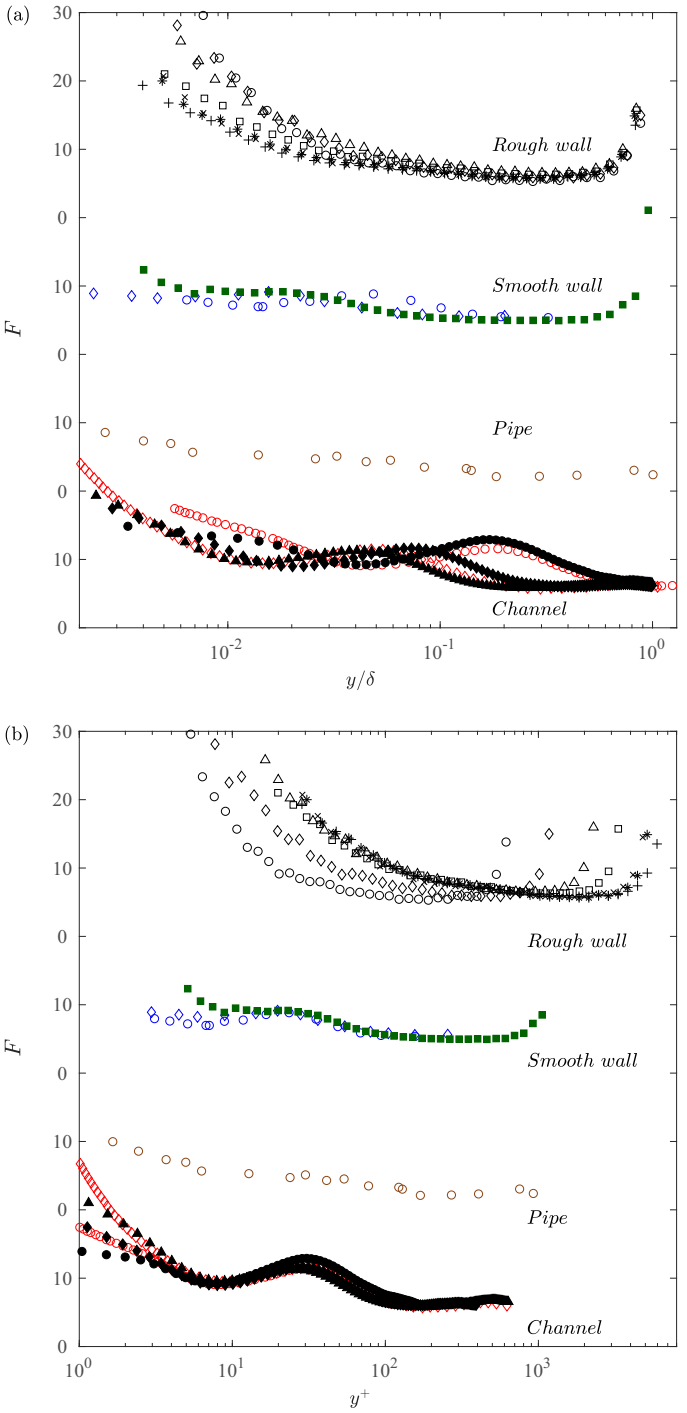

FIG. 2. Flatness factor of the velocity derivative F in a pipe, channel flow, and turbulent boundary layers as a function of (a) y/δ and (b) y^+. Symbols are as in Fig. 1. Note that the data for the pipe, and smooth and rough wall turbulent boundary layers are plotted using multiple ordinate axes for clarity.

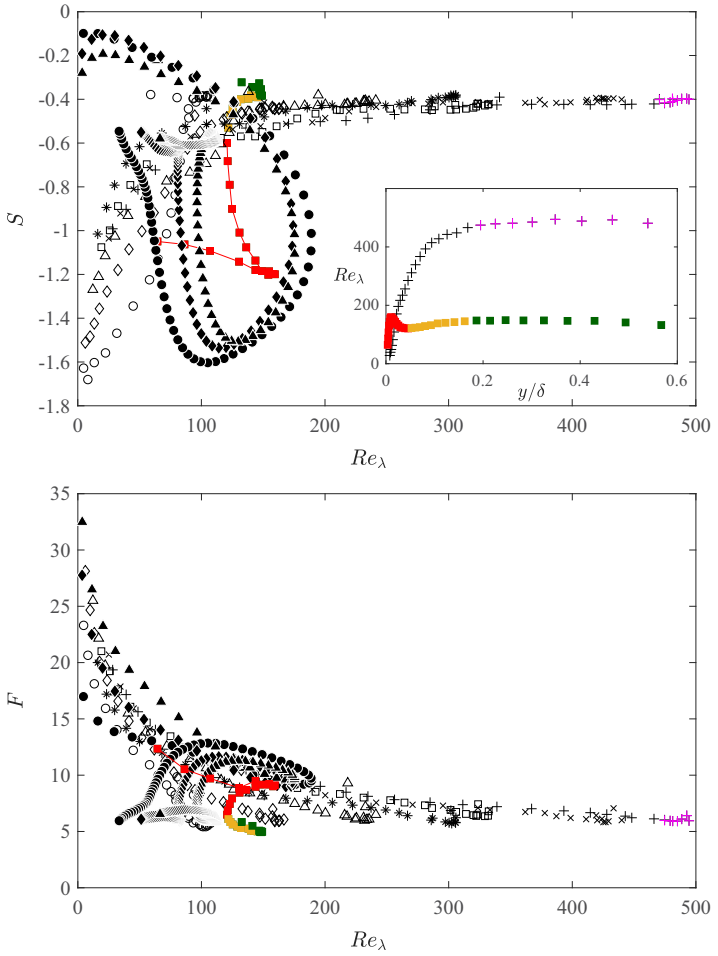

FIG. 3. Distributions of S and F as a function of Re_λ. Symbols are the same as in Fig. 1, except for the smooth wall data and $\mathrm{Re}_\tau = 7170$ data of the rough wall. The smooth wall boundary layer data are color coded as three regions: near-wall region (red, $y/\delta \leqslant 0.04$), inertia-dominated region (yellow, $0.04 \leqslant y/\delta \leqslant 0.2$), and outer region (green, $0.2 \leqslant y/\delta \leqslant 0.6$). For the rough wall data, data in the outer region, $0.2 \leqslant y/\delta \leqslant 0.6$, are shown in magenta. Inset: Re_λ profiles of smooth wall and rough wall ($\mathrm{Re}_\tau = 7170$) with similar color coding as in the S distributions.

flows. The message conveyed by Figs. 1–3 is clear: S and F can vary significantly from location to location within a given nonhomogeneous turbulent flow, while they can be independent of Re_λ in some parts of the flow. Accordingly, the uncertainty of the measurement locations can lead to quite different conclusions on the magnitudes of S and F and their dependencies on Re_λ. Thus, considering the large uncertainty in the value of y/δ for the ASL measurements, caution must be exercised, even though these measurements are at Reynolds numbers that are much higher than those obtained in a laboratory. To illustrate this point, we report in Fig. 5 the values of S obtained in the ASL by Refs. [21,22] with the present data measured in the smooth and rough wall turbulent boundary layers. The original data reported by Ref. [21] used values of Re_λ based on an arbitrarily definition, i.e., $\mathrm{Re}_{\lambda,\mathrm{WT}} = w'\lambda/\nu$, where w' is the vertical velocity rms. Reference [23] proposed a correction for $\mathrm{Re}_{\lambda,\mathrm{WT}}$ and arbitrarily multiplied by a factor 2.5. It is these later "corrected" data which are reported in Ref. [4]. These data were collected at distances from the wall $y = 5.66, 11.3,$

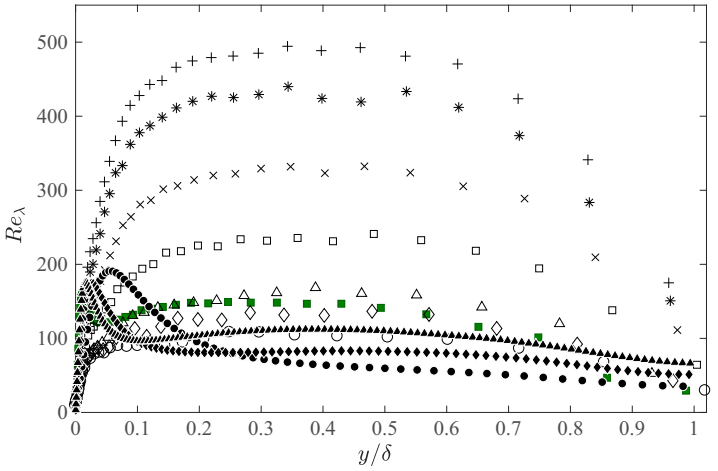

FIG. 4. Comparison of Re_λ profiles at different streamwise locations in smooth and rough wall boundary layers; see Table I for symbols representing the smooth wall and rough wall data. Solid symbols: Present DNS of smooth wall channel flow.

and 22.6 m. Unfortunately, Ref. [21] did not show the distribution of S as a function of y, which makes it impossible to identify the data taken at the respective positions of y. The data of Ref. [22] are measured at a height of 108 m about the ground with a hot-wire probe mounted on a wing of a plane. Measurements were acquired on different days, 1 July 1968 (12:00 pm–13:11 pm) and 28 July 1968 (11:32 pm–21:45 pm). Notice the significant difference in the values of S between the two series of data. On average, the magnitudes of S of the data measured on 28 July 1968 are quite low, either due to error measurements or, most likely, a change in the ASL conditions from those of 1 July 1968. Since one expects that the neutral ASL can be treated as a turbulent boundary layer where S, F, and Re_λ vary in a nontrivial manner as shown here, one should take caution in inferring the Reynolds number dependency of S and F based on a few measurements acquired in the ASL in the vicinity of the ground [21] or ocean [24]. It is interesting to note that the values of $-S$ at $y = 108$ m

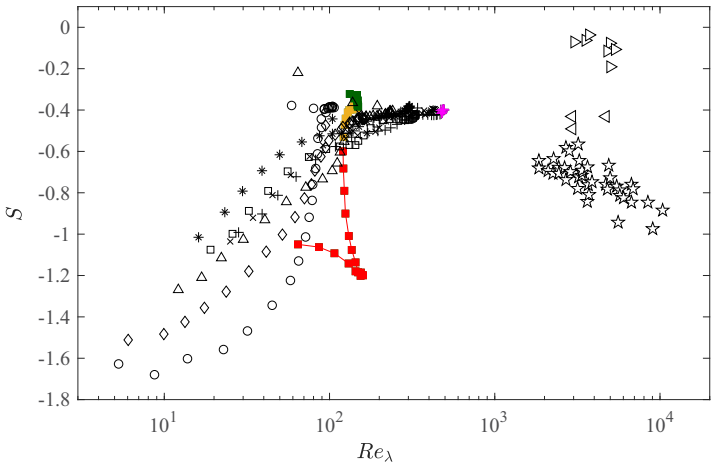

FIG. 5. Distributions of S as a function of Re_λ in laboratory turbulent boundary layer and ASL. Symbols are the same as in Fig. 3 for the smooth wall and rough wall boundary layers. ASL data: ☆ [21], and ◁ (28 July 1968) and ▷ (1 July 1968) [22].

measured by Ref. [22] on 1 July 1968 agree relatively well with that in the region of the boundary layer where S and Re_λ are constant simultaneously, while the measurements of Ref. [21] and those reported in Ref. [4] from other results at a much lower height show a different trend. This shows that one must first determine the actual y/δ location of the ASL data and ascertain if the data are free of any near-wall effects before including them in any assessment of K41 and K62. The multivaluedness of S and F at given Re_λ, well illustrated in Figs. 3 and 5, highlights the ambiguity that can arise if such data are used without a precise knowledge of y/δ. Alternatively, the inset of Fig. 3 suggests a relatively simple and objective criterion for measuring both S and F free of near-wall effects: Re_λ should be constant over a non-negligible range of y (and maximum). As stated above, one can then expect the local isotropy to be well approximated in this region. Thus, if the Reynolds number is large enough, according to Ref. [25], the transport equation for the enstrophy (ω^2) reduces to $P_\omega = D_\omega$, where P_ω and D_ω are the production by vortex stretching and destruction by the effect of viscosity, respectively, of ω^2. The balance between P_ω and D_ω indicates that the small scales have reached an energy equilibrium which is consistent with constant Re_λ, S, and F. Consequently, the two requirements (i.e., local isotropy and high Re_λ) to test K41 and/or K62 are most likely to be met in that region. Interestingly, the ALS data reported in Ref. [4] were measured at heights no larger than 40 m, and thus are most likely to fall in the lower part of the log region of the mean velocity profile. In this region the balance between turbulent energy production and dissipation is not well verified.

IV. CONCLUDING DISCUSSION

We have carried out hot-wire measurements in laboratory turbulent boundary layers (LTBLs) over smooth and rough walls, with the assumption that such flows may have similar features to those for a neutral ASL. We also analyzed data from direct numerical simulations of a smooth wall turbulent channel flow.

The LTBL measurements of S and F indicate that, as the distance to the wall (y) increases, both S and F vary significantly before approaching a constant in some part of the outer layer. It is observed that Re_λ varies strongly with y before becoming approximately constant in the region $0.3 \leqslant y/\delta \leqslant 0.6$. A similar behavior for S, F, and Re_λ is observed in the channel flow DNS data.

The results show that caution is needed when using measurements in wall shear flows, such as boundary layers, and pipe and channel flows for the purpose of testing K41 and K62. One must ensure that, in addition to the requirement of a very high Reynolds number (a necessary but insufficient condition) and local isotropy, the measurements should be carried out in the region of the flow where S, F, and Re_λ are independent of the distance to the wall. The present study suggests that the region $0.3 \leqslant y/\delta \leqslant 0.6$ may be adequate for this purpose.

If one accepts that the laboratory turbulent boundary layer is an adequate surrogate for the neutral ASL, then the behavior of S and F in the ASL is expected to be similar to that reported in this study. This raises concerns regarding the use of the ASL data reported in Ref. [4] for testing K41 and K62. Indeed, they have usually been obtained at relatively small heights, typically below 30 m. If we assume that the thickness of the ASL is about 100 m (a conservatively low figure considering that the general consensus is that the thickness of the ASL is about 10% of the planetary boundary layer, which can extend to at least 2 km) the ASL data fall in the region $y/\delta \leqslant 0.3$, which does not comply with the present recommendation. The behavior of S and F reported in this study illustrates the concerns raised [26] with regard to the use of ASL data for testing the consequences of K41 and K62.

ACKNOWLEDGMENT

The Australian Research Council (ARC) is gratefully acknowledged for the financial support of this work.

[1] A. N. Kolmogorov, The local structure of turbulence in incompressible viscous fluid for very large Reynolds numbers, Dokl. Akad. Nauk SSSR **30**, 301 (1941).
[2] A. N. Kolmogorov, Dissipation of energy in locally isotropic turbulence, Dokl. Akad. Nauk SSSR **32**, 16 (1941).
[3] A. N. Kolmogorov, A refinement of previous hypotheses concerning the local structure of turbulence in a viscous incompressible fluid at high Reynolds number, J. Fluid Mech. **13**, 82 (1962).
[4] K. Sreenivasan and R. A. Antonia, The phenomenology of small-scale turbulence, Annu. Rev. Fluid Mech. **29**, 435 (1997).
[5] A. S. Monin and A. M. F. Obukhov, Basic laws of turbulent mixing in the surface layer of the atmosphere, Contrib. Geophys. Inst. Acad. Sci. USSR **151**, e187 (1954).
[6] J. C. Wyngaard, Atmospheric turbulence, Annu. Rev. Fluid Mech. **24**, 205 (1992).
[7] M. Metzger, B. J. McKeon, and H. Holmes, The near-neutral atmospheric surface layer: Turbulence and non-stationarity, Philos. Trans. R. Soc., A **365**, 859 (2007).
[8] N. Hutchins, K. Chauhan, I. Marusic, J. Monty, and J. Klewicki, Towards reconciling the large-scale structure of turbulent boundary layers in the atmosphere and laboratory, Boundary-Layer Meteorol. **145**, 273 (2012).
[9] H. Ueda and J. O. Hinze, Fine-structure turbulence in the wall region of a turbulent boundary layer, J. Fluid Mech. **67**, 125 (1975).
[10] M. Elena, Suction effects on turbulence statistics in a heated pipe flow, Phys. Fluids **27**, 861 (1984).
[11] A. W. Vreman and J. G. M. Kuerten, Statistics of spatial derivatives of velocity and pressure in turbulent channel flow, Phys. Fluids **26**, 085103 (2014).
[12] O. Oyewola, L. Djenidi, and R. A. Antonia, Combined influence of the Reynolds number and localised wall suction on a turbulent boundary layer, Exp. Fluids **35**, 199 (2003).
[13] K. A. Chauhan, H. M. Nagib, and P. A. Monkewitz, Criteria for assessing experiments in zero pressure gradient boundary layers, Fluid Dyn. Res. **41**, 021404 (2009).
[14] P.-Å Krogstad, R. A. Antonia, and L. W. B. Browne, Comparison between rough- and smooth-wall turbulent boundary layers, J. Fluid Mech. **245**, 599 (1992).
[15] Md. Kamruzzaman, L. Djenidi, R. A. Antonia, and K. M. Talluru, Drag of a turbulent boundary layer with transverse 2D circular rods on the wall, Exp. Fluids **56**, 1 (2015).
[16] K. M. Talluru, V. Kulandaivelu, N. Hutchins, and I. Marusic, A calibration technique to correct sensor drift issues in hot-wire anemometry, Meas. Sci. Technol. **25**, 105304 (2014).
[17] H. Abe, R. A. Antonia, and H. Kawamura, Correlation between small-scale velocity and scalar fluctuations in a turbulent channel flow, J. Fluid Mech. **627**, 1 (2009).
[18] Y. Morinishi, T. S. Lund, O. V. Vasilyev, and P. Moin, Fully conservative higher order finite difference schemes for incompressible flow, J. Comput. Phys. **143**, 90 (1998).
[19] S. Hoyas and J. Jiménez, Reynolds number effects on the Reynolds-stress budgets in turbulent channels, Phys. Fluids **20**, 101511 (2008).
[20] P. Mestayer, Local isotropy and anisotropy in a high-Reynolds-number turbulent boundary layer, J. Fluid Mech. **125**, 475 (1982).
[21] J. C. Wyngaard and H. Tennekes, Measurements of the small-scale structure of turbulence at moderate Reynolds numbers, Phys. Fluids **13**, 1962 (1970).
[22] C.-M. Sheih, H. Tennekes, and J. L. Lumley, Airborne hot-wire measurements of the small-scale structure of atmospheric turbulence, Phys. Fluids **14**, 201 (1971).
[23] C. W. Van Atta and R. A. Antonia, Reynolds number dependence of skewness and flatness factors of turbulent velocity derivatives, Phys. Fluids **23**, 252 (1980).
[24] C. H. Gibson, G. R. Stegen, and R. B. Williams, Statistics of the fine structure of turbulent velocity and temperature field at high Reynolds number, J. Fluid Mech. **41**, 153 (1970).
[25] H. Tennekes and J. L. Lumley, *A First Course in Turbulence* (MIT Press, Cambridge, MA, 1974).
[26] R. A. Antonia, S. L. Tang, L. Djenidi, and L. Danaila, Boundedness of the velocity derivative skewness in various turbulent flows, J. Fluid Mech. **781**, 727 (2015).